Supplementary Materials for

Intravital Imaging of Mouse Embryos

Qiang Huang*#, Malkiel A. Cohen*, Fernando C. Alsina, Garth Devlin, Aliesha Garrett, Jennifer McKey, Patrick Havlik, Nikolai Rakhilin, Ergang Wang, Kun Xiang, Parker Mathews, Lihua Wang, Cheryl Bock, Victor Ruthig, Yi Wang, Marcos Negrete, Chi Wut Wong, Preetish K.L. Murthy, Shupei Zhang, Andrea R. Daniel, David G. Kirsch, Yubin Kang, Blanche Capel, Aravind Asokan, Debra L. Silver, Rudolf Jaenisch#, Xiling Shen#

*These authors contributed equally to this work.

#Correspondence to: drhuang@xjtu.edu.cn, jaenisch@wi.mit.edu, xiling.shen@duke.edu

This PDF file includes:

Other Supplementary Materials for this manuscript include the following:

Materials and Methods

Ethics statement

All animal procedures were reviewed and approved by the Institutional Animal Care and Use Committee (IACUC) of Duke University (Protocol Nos. A195-15-06 2015-2018 and A139-18-05 2018-2021) or by the Committee on Animal Care (CAC) and the Department of Comparative Medicine (DCM) at the Massachusetts Institute of Technology (Protocol #0916-058-18), and were conducted in accordance with National Institutes of Health guidelines.

Animal models

Wnt1-cre;tdTomato mice were generated by crossing Tg(Wnt1-cre)11Rth/Tg(Wnt1-GAL4)11Rth/J mice (Jackson Laboratory: 003829) with Ai14 mice (Jackson Laboratory: 007914). C57BL/6, C57BL/6-Tg(CAG-RFP/EGFP/Map1lc3b)1Hill/J and C57BL/6J-Tg(Thy1-GCaMP6s)GP4.3Dkim/J mice were obtained from Jackson Laboratory (000664, 027139 and 024275). The Lgr5-DTR-eGFP mouse was obtained from the de Sauvage lab at Genentech. All chimeric injections were performed in CD1 mice. CD1 mice were obtained from Charles River Laboratories.

3-D printing of window and clip

The windows and clip were designed using AutoCAD 2016 (AutoDesk). The window frames were 3D-printed titanium (Materialise) and cover glasses were cut from borosilicate heat-resistant UV fused-silica glass (Mark Optics, Corning 7980) with a 30W CO2 laser (Epilog, Zing). The clip was printed by a Ultiamaker 2+ 3D printer.

Surgical procedure

Pregnant female mice were anesthetized using 2% isoflurane with oxygen at 2 L/min. The abdomen was shaved and cleaned with 70% ethanol and iodine. After covering with a sterile field,

a round incision was made in the abdomen, removing some of the skin. A midline incision was then made in the abdominal muscle and embryos were removed from the abdominal cavity. An embryo close to the ovary was selected, the optical window was implanted, the embryo was sutured to the abdominal muscle, and the abdominal muscle was sutured to the window. For embryos before E12.5, a small incision was made by scissors, and the uterine muscle was stripped with forceps to make a round incision. Then the decidua was removed by dipping with wet applicators. The incision was closed by attaching the window frame to the skin using glue.

In vivo and *in vitro* multiphoton imaging

In vivo imaging was performed using a Leica SP8 two-photon DIVE or Zeiss Lumar.V12 stereoscope. For the stereoscope, fluorescence emission was collected in two channels: 515–565 nm for detection of eGFP, and 575–640 nm for detection of tdTomato. For the multiphoton system, the eGFP excitation wavelength was 920, the tdTomato excitation wavelength was 1050 nm, the mCherry excitation wavelength was 1080 nm, and the RFP excitation wavelength was 1085 nm. The objective used to visualize cells *in vivo* was a 25x/1.05 NA water immersion objective with a motorized correction collar; WD 1.8 mm. Mice were placed on a 3D-printed imaging stage with eye ointment and anaesthetized with isoflurane (3% v/v with 2% maintenance). For *in vitro* imaging, embryos were fixed in 4% paraformaldehyde for 24 h and embedded in phosphate-buffered saline during observation.

Whole embryo staining

Embryos were fixed in 4% paraformaldehyde for 24 h and incubated with Anti-Mouse CD31 (1:200, BD bioscience, Cat#553370) or Anti-PDGFR beta (1:100, Abcam, Cat#aba32570) at 4℃ with gentle rotation for 72 h. Donkey Anti-Mouse IgG H&L (Alexa Fluor® 488) (1:500,

Abcam, Cat#150105) or Donkey Anti-Rabbit IgG H&L (Alexa Fluor® 488) (1:500, Abcam, Cat#ab150073) was applied as secondary antibody at 4℃with gentle rotation for 48 h.

Recombinant virus production and titers

HEK293 cells were cultured in DMEM supplemented with 10% fetal bovine serum (FBS) (Sigma Aldrich) and 1% penicillin-streptomycin (P/S; Thermo Fisher) in 5% CO_2 at 37°C. Recombinant AAV vectors were produced using a triple plasmid transfection method, using an AAV plasmid (pXR8g9, encoding AAV2 replication proteins and a chimeric AAV8-derived capsid engrafted with galactose binding residues derived from AAV9), an adenoviral helper plasmid (pXX680), and a transgene packaging cassette, encoding either self-complementary GFP driven by a chicken beta actin hybrid promoter (pTR-CBh-scGFP) or single-stranded RFP driven by the chicken beta actin promoter (pTR-CBA-td-tomato), flanked by AAV2 inverted terminal repeat (ITR) sequences. Viral vectors were purified via iodixanol density gradient ultracentrifugation, subjected to phosphate-buffered saline (PBS) buffer exchange using Zeba Spin 40 kDa molecular weight cut-off (MWCO) desalting columns (Thermo Fisher 87772). Titers of purified virus preparations were determined by quantitative PCR with primers amplifying the AAV2 ITR regions (forward, 5′ AACATGCTACGCAGAGAGGGAGTGG-3′; reverse, 5′-CATGAGACAAGGAACCCCTAGTG ATGGAG-3′) (IDT Technologies, Ames IA).

Fluorescein and AAV injection

Fluorescein (10 mg/kg, Sigma-Aldrich, Cat# F2456) was injected through the orbital vein after implanting the optical window at E15.5. AAVs (2.5×10^{11}) were injected through the dam tail vein at E11.5 and the window was implanted at E14.5.

In utero electroporation

In utero electroporation was performed as described previously (*39, 40*). Briefly, E13.5 or E14.5 pregnant females were anesthetized using isoflurane. An incision in the abdomen was made and the uterine horns were exposed. Each embryo was injected with 1-1.5 µl of plasmid solution (0.01% fast green and 0.9 µg/µl pCAG-EGFP or 0.9 ug/ul pCAG-mCherry) and electroporated using five 50 ms pulses at 40 V with a pulse interval of 950 ms, using platinum-plated BTX Tweezertrodes. Uterine horns were repositioned into the abdominal cavity and the muscle and skin incisions were sutured. IACUC procedures were followed to ensure appropriate care and anesthesia of the animals. The following day, the window was implanted in the dam and the electroporated hemisphere of one embryo was imaged using two-photon microscopy. Imaging of electroporated area was repeated at 24 h after window implantation.

Cultures of mESCs and their differentiation into mNCCs

C57Bl/6;*R26*$^{(tdTomato/M2rtTA)}$ and C57Bl/6;*Col1a1*$^{(GFP)}$ mESCs (*38*) were cultured as previously described (*41, 42*), then plated and differentiated in DMEM:F12 N2/B27 medium on laminin/fibronectin-coated dishes for 8 d. bFGF (20 ng/mL; Peprotech) was applied in the first 4 d; bFGF and BMP4 (10 ng/mL; Peprotech) were added in the following 4 d.

Cultures of hPSCs and their differentiation into hNCCs

AAVS1$^{(CAAGS::GFP)}$ hPSCs were cultured as described previously (*43*) on inactivated MEF feeders in DMEM/F12 medium supplemented with 15% v/v FBS (HyClone), 5% v/v KOSR (Invitrogen), 0.1 mM beta-mercaptoethanol (Sigma-Aldrich), 1% P/S, 1 mM L-glutamine (Invitrogen), 1% NEAAs (Invitrogen), and 4 ng/mL bFGF (Peprotech), and were differentiated to

NCCs as described previously (*44, 45*). Stemgent SB431542 (10 μM) and LDN193189 (500 nM) were used for neural induction for 3 d, and Stemgent CHIR99021 (3 μM) was used for further differentiation for 8 d. N2B27 supplemented with bFGF and EGF (both at 20 ng/mL) was used for culturing hNCCs.

Microinjection into pre-implantation E2.5 embryos

Female Hsd:ICR(CD-1) Envigo mice were naturally mated to male mice and the copulation plug was noted at 0.5 d post coitum (dpc). At 2.5 dpc, 8 embryos were harvested by oviduct flushing of female embryo donors. Eight cell-stage through morulae-stage embryos were injected, one-by-one, with ~10 mESCs each. After injection, embryos were incubated overnight in drop culture in KSOM medium under oil. After overnight culture, injected embryos were transferred into the uterus of a 2.5-dpc pseudopregnant recipient. Embryo harvest and transfer surgeries were performed in accordance with Duke University Institutional Animal Care and Use Program protocols.

Microinjection into mid-gestation E8.5 embryos

Microinjections of NCCs were performed as previously described (*36,37*). Laparotomy of E8.5 pregnant females was performed by a long, vertical incision and the uterus was exposed. Cells (hNCCs and mNCCs in a 1:2 ratio) were drawn into a glass micropipette and injected into the distal third of the decidual swelling. Roughly, 2-5 x 10^3 cells (suspended in 0.25-0.75μL of cell culture media) were injected per embryo.

Statistics and image analysis

Statistical analysis was performed using the SPSS 18.0 statistical package. Student's T-test was used to compare the parameters between embryos or mice with and without the window.

tdTomato(+) and GFP(+) cells after injection of AAVs were observed in 10 random fields for each animal. Data are presented as mean±SD. $P<0.05$ was defined as statistically significant.

Image analysis

Images were processed by ImageJ. Cell tracking was preformed using Imaris 9.5.0 with the Imaris for Tracking Package (Oxford Instruments). We first processed the video using translational correction to stabilize motion artifacts, preserving the total area captured. Objects were identified using spot generation with a target size of 15 μM and a quality of 22 of greater. Tracks for each object were followed through the entire recording. Finally, a stationary object was identified for a final track correction; this reference track was utilized to perform a final compensation step for motion artifacts not completely rectified during initial stabilization.

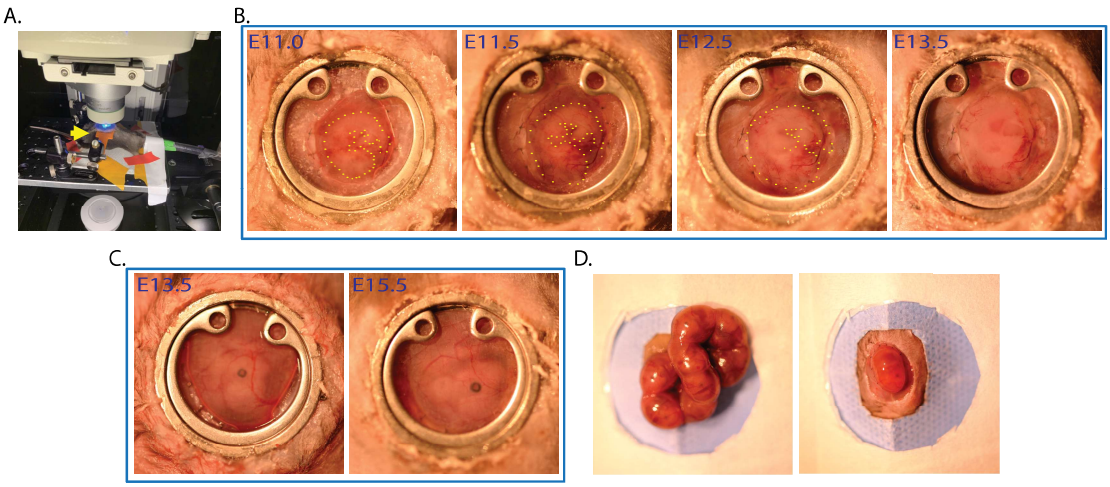

Fig.S1. Surgical procedure. (**A**). A 3D-printed clip (Yellow arrow) was used to stabilize the window. (**B**). The embryo was alive and growing after the stripping of the decidua and uterine muscle and the implantation of the window performed at E11. The imaged embryo retracted towards the mother abdominal cavity by E13.5. (**C**). The same embryo was adjusted with a new window to continue observation. (**D**). The decidua diminished and the uterine wall became transparent, allowing observation after E12.5.

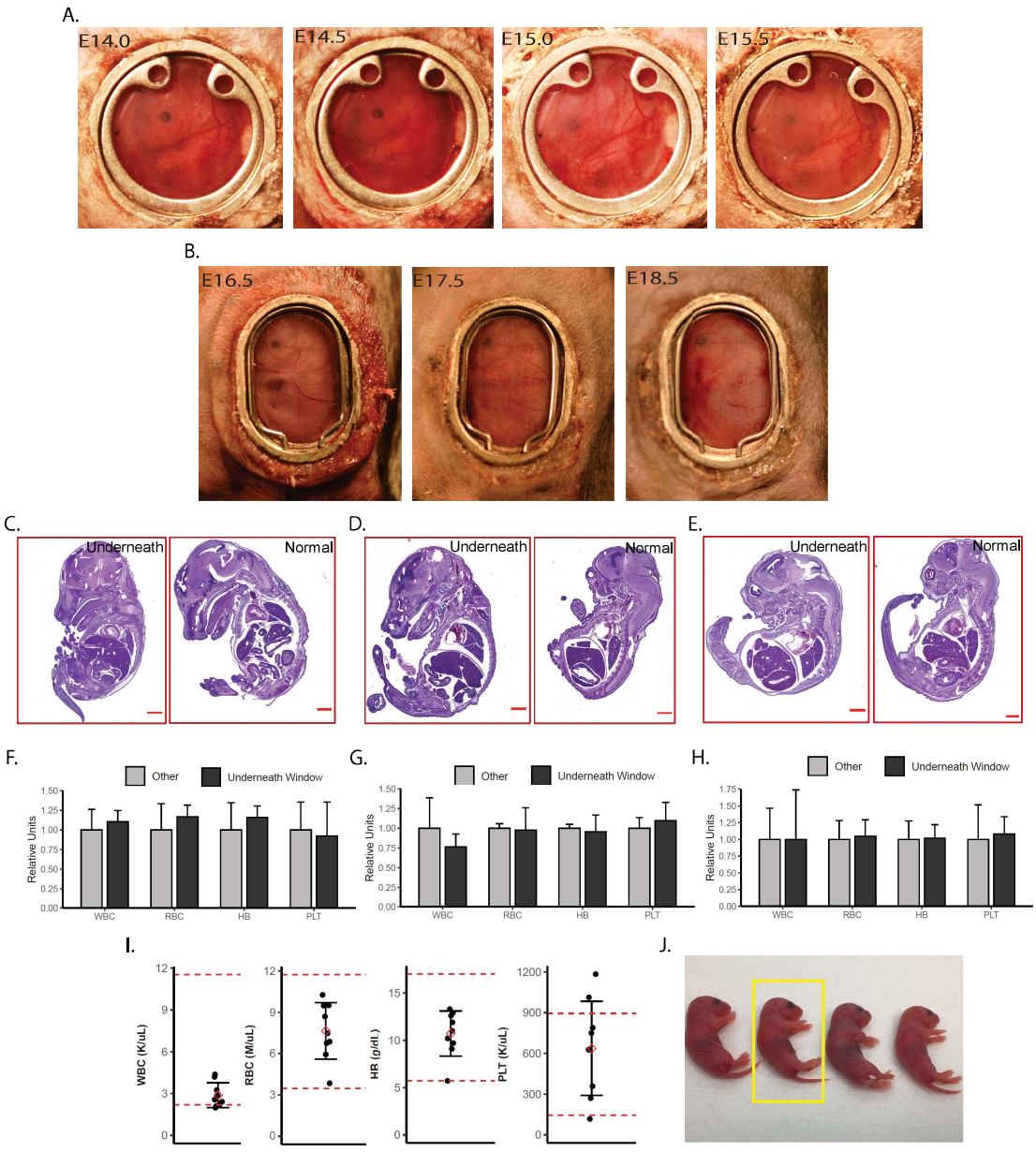

Fig.S2. Survival of embryos after window implantation. (**A**). Series of light field views throughout 36 hours of an embryo development, after implanting a window at E14.0. (**B**). Series of light field views throughout 48 hours of an embryo development, after implanting the larger elliptical window at E16.5. (**C-E**). H&E staining of embryos underneath the window compared with littermate embryos at E14.5 (3 days after stripping surgery performed at E11.5) (**C**), at E15.5 (3 days after non-stripping surgery performed at E12.5) (**D**), and at E18.5 (3 days after non-

stripping surgery performed at E15.5) (**E**). Scale bar, 1 mm. (**F-H**). Complete blood components of embryos underneath the window compared with littermate embryos at E14.5 (3 days after stripping surgery) (**F**), at E15.5 (3 days after non-stripping surgery) (**G**), and at E18.5 (3 days after non-stripping surgery) (**H**). Data are mean ± SD. (**I**). Complete blood components of the dams, 3 days after surgery (n=3 with stripping surgery, n=6 with non-stripping surgery: 3 with circular windows, 3 with elliptical windows). The red dash lines indicate the normal range (*46*). Data are mean ± SD. (**J**). The embryos were delivered normally and survived birth. The labeled one was underneath the window (P0).

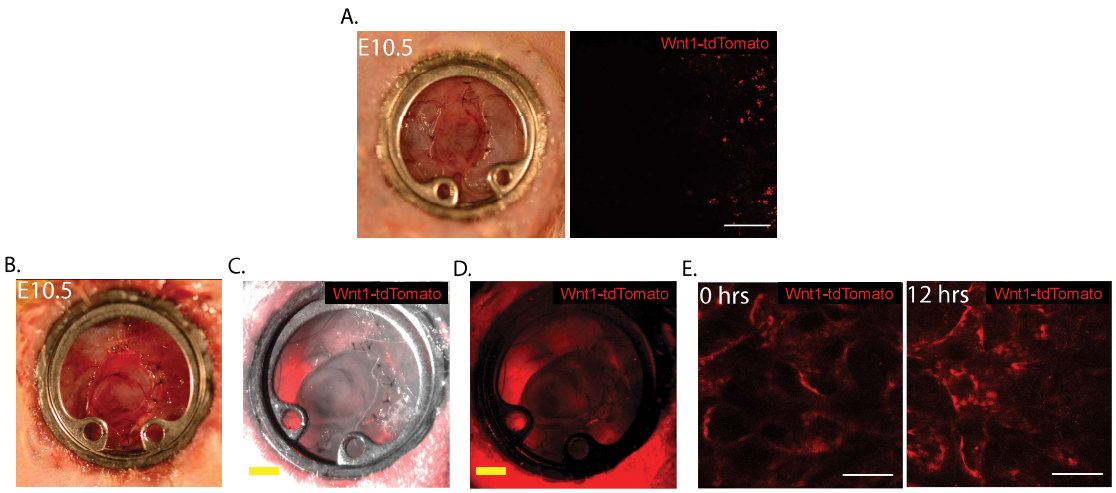

Fig.S3. ***In vivo*** **two-photon microscopy.** (**A**). Light-field and two-photon images of a wnt1-cre:tdTomato mouse embryo without stripping the decidua and uterus muscle at E10.5. Limited tdTomato signals were detected. Scale bar, 100 µm. (**B-D**). View of a Wnt1-cre:tdTomato mouse embryo after implanting the window and stripping the decidua and uterus muscle at E10 using a stereoscopic microscope. The specific brain region depicted in panel E is indicated by the yellow square. (B- brightfield; C.- Overlay; D- tdTomato, Scale bar, 2 mm). (**E**). Two-photon imaging of Wnt1-cre; tdTomato mouse embryo after stripping at E10.5 (0 hours) and at E11.0 (12 hours). Scale bar, 100 µm.

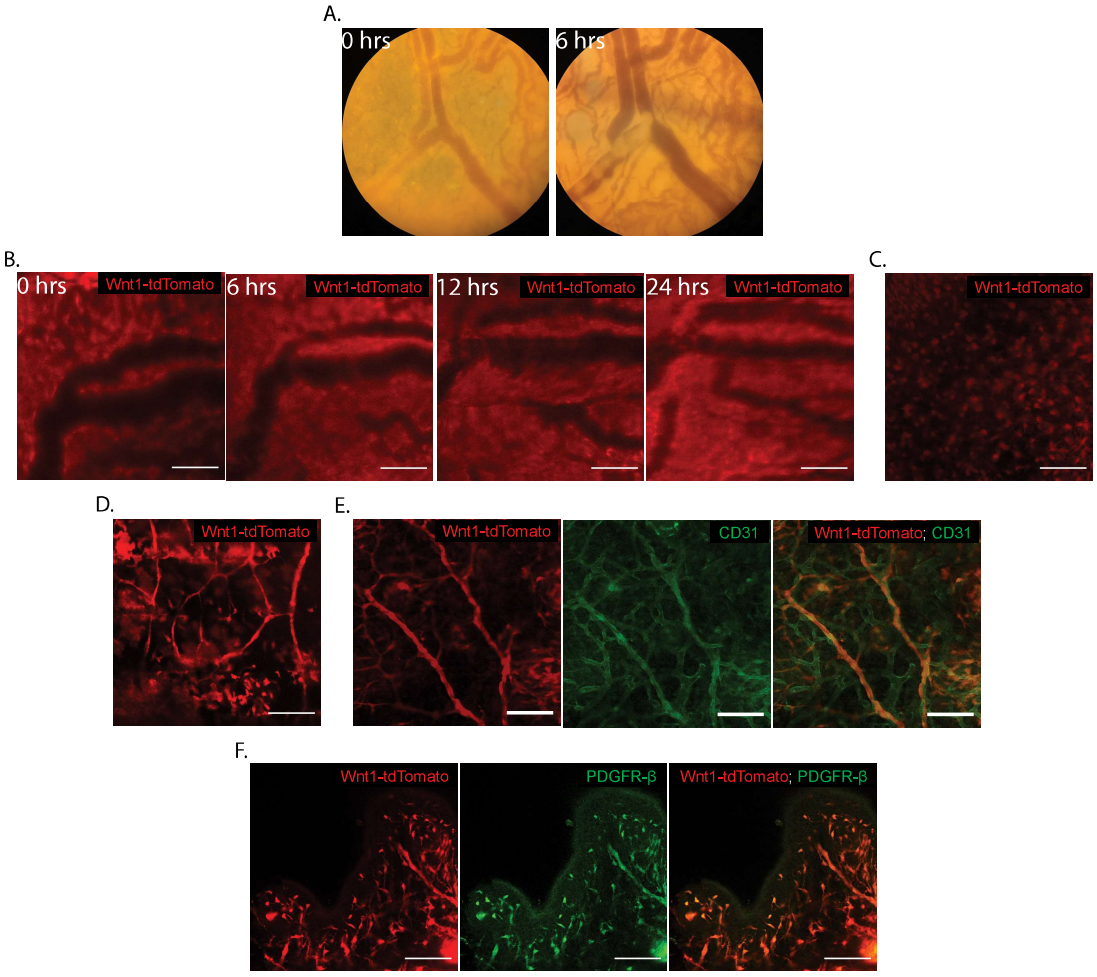

Fig.S4. Vasculature on the uterine surface and in the brain. (**A**). Uterine surface vasculature used as a roadmap during continuous imaging. (**B**). Embryonic brain vasculature used as a roadmap during imaging. Scale bar, 100 µm. (**C**). *In vitro* Wnt1-positive neurons from a fixed E14.5 embryo. (**D**). Mesh-like layer in a Wnt1-cre:tdTomato mouse embryo brain imaged using two-photon microscopy. Scale bar, 100 µm. (**E**). Mesh-like layer stained with anti-CD31 antibody, showing CD31-positive vasculature. Scale bar, 100 µm. (**F**). Mesh-like layer stained with anti-PDGFR-β antibody, indicating that this structure was also PDGFR-β-positive. Scale bar, 100 µm.

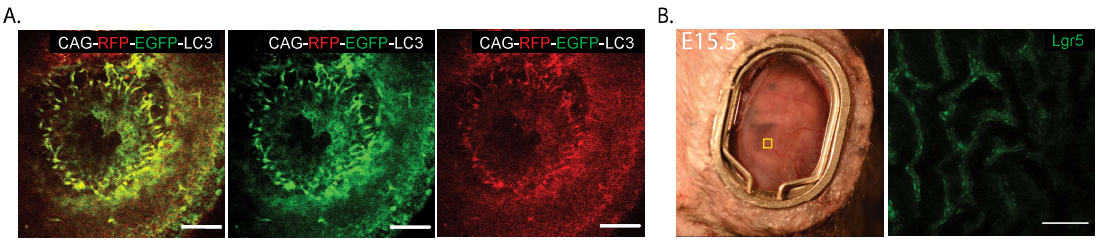

Fig.S5. Images of CAG-RFP-EGFP-LC3 embryo and Lgr5-DTR-eGFP embryo. (**A**). *In vitro* images of a retina of a CAG-RFP-EGFP-LC3 mouse embryo at E15.5. (**B**). *In vivo* images of the intestine of a Lgr5-DTR-eGFP embryo at E 15.5. Scale bar, 100 μm.

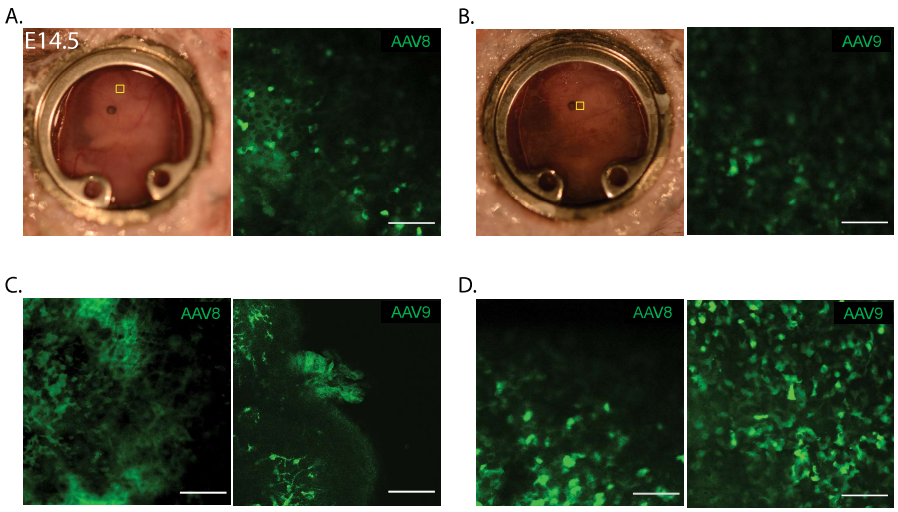

Fig.S6. GFP expression in embryos following dam tail vein injection of rAAVs. (**A-B**). Images from an embryo at 72 h after injection of (**A**) AAV8g9-pTR-CBh-scGFP, at E14.5, and (**B**) AAV9-pTR-CBh-scGFP, at E14.5. (**C**). Images of the embryos in dams without the windows at 72 h after injection of AAV8g9-pTR-CBh-scGFP or AAV9-pTR-CBh-scGFP at E14.5. (**D**). Images for the placenta at 72 h after injection of AAV8g9-pTR-CBh-scGFP or AAV9-pTR-CBh-scGFP at E14.5. Scale bar, 100 μm.

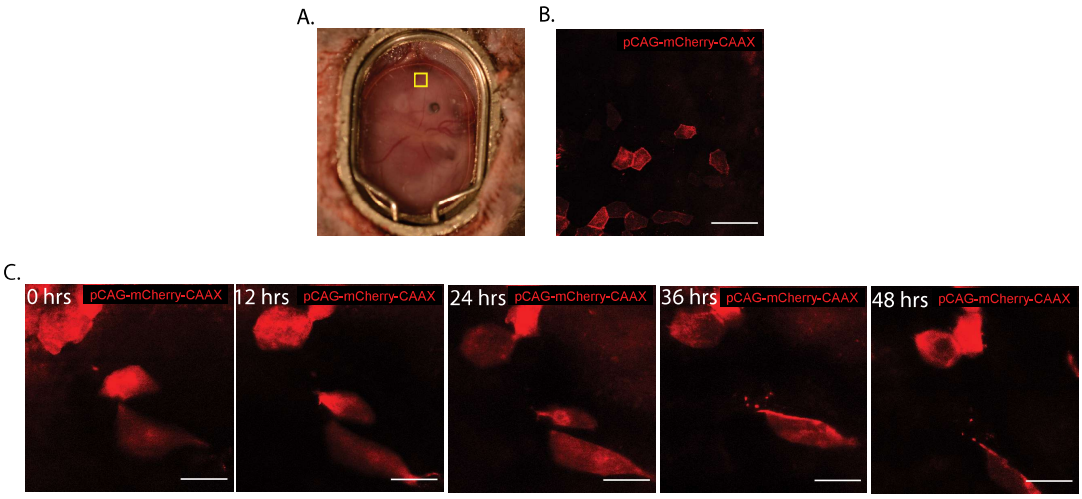

Fig.S7. Imaging of neurons following *in utero* electroporation of a membrane marker. (**A**). Light field view of an E16.5 embryo three days after electroporation of pCAG-mCherry-CAAX. (**B**). Cells expressing membrane-bound mCherry in the specific brain region (yellow square) depicted in panel A. (**C**). Imaging of the labeled neurons for 48 hours in the brain. Scale bar, 100 µm.

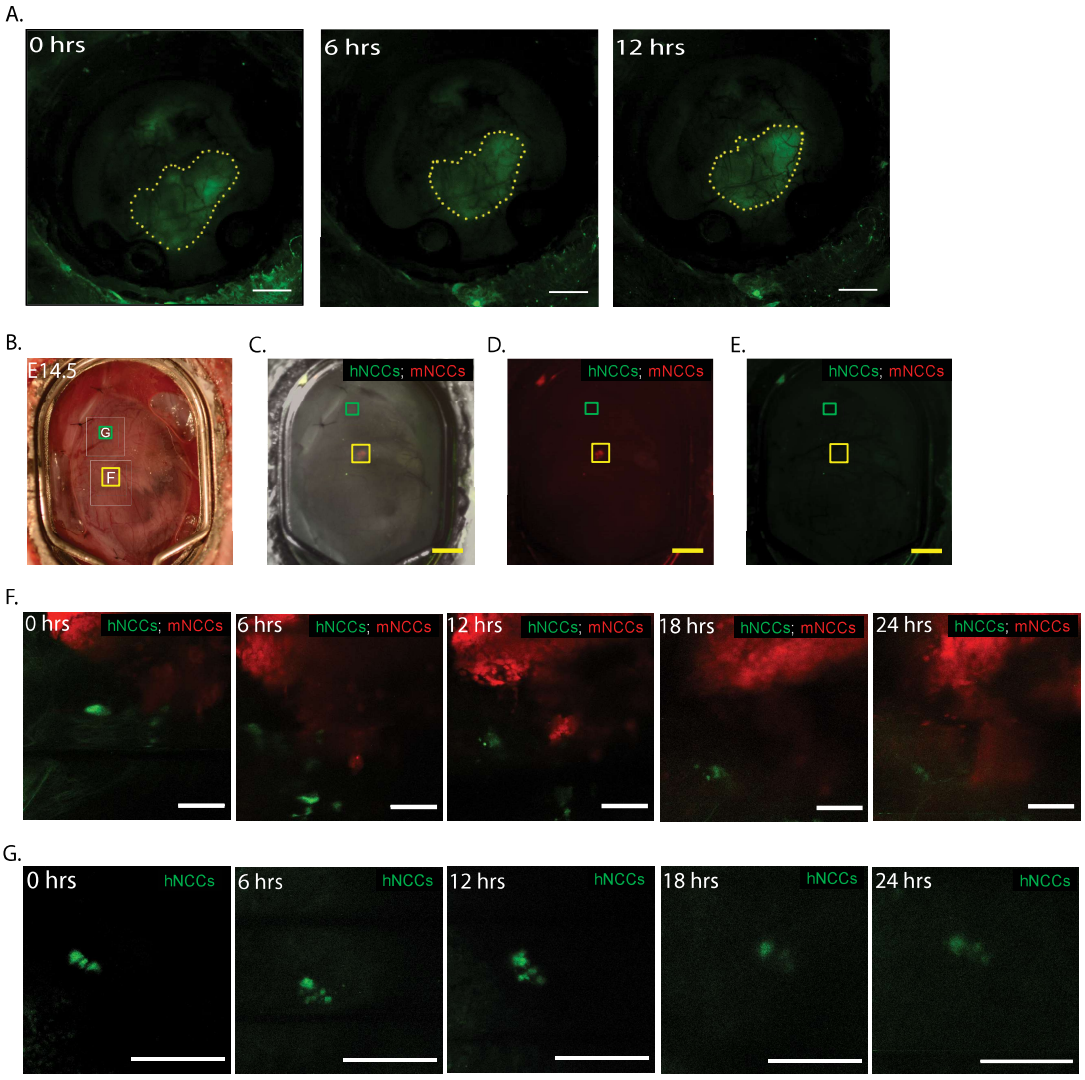

Fig.S8(1). Chimeras injected with mESCs or hNCCs and mNCCs at different embryo stages. (**A**). Continuous observation of a whole blastocyst-chimeric embryo injected with GFP+ mESCs for 12 hours, using stereoscopic microscopy. Scale bar, 2 mm. (**B-E**). Light-field (**B**), overlay (**C**), tdTomato (**D**), and eGFP (**E**) view of a chimeric embryo that was co-injected with GFP+ hNCCs and tdTomato+ mNCCs at E8.5. Window was placed at E14.5. The embryonic regions depicted in panels F and G are indicated by the yellow and green squares. Scale bar, 2 mm. (**F**). 24-hour two-photon imaging of a NC chimeric embryo containing both hNCCs (GFP+) and mNCCs (tdTomato+). Scale bar, 100 μm. (**G**). 24-hour two-photon imaging (starting E14.5) of a NC chimeric embryo containing individual GFP+ hNCCs. Scale bar, 100 μm.

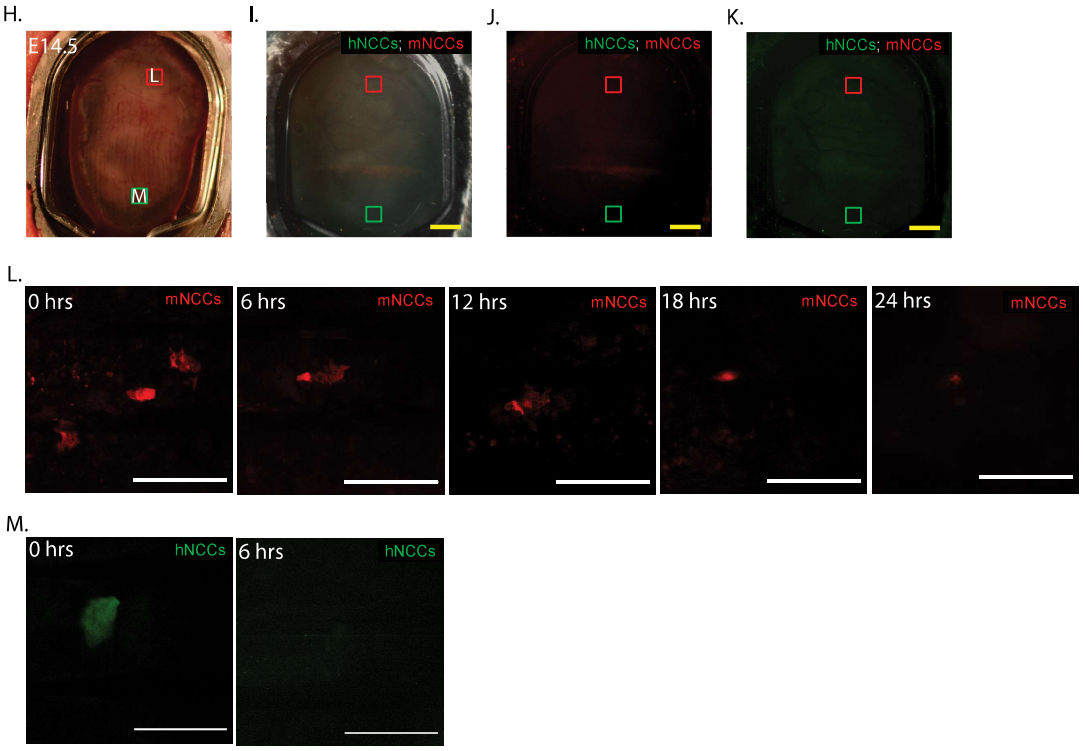

Fig.S8(2). Chimeras injected with mESCs or hNCCs and mNCCs at different embryo stages. (**H-K**). Light-field (**H**), overlapped (**I**), tdTomato (**J**), and EGFP (**K**) view of a chimeric embryo that was co-injected with GFP+ hNCCs and tdTomato+ mNCCs at E8.5. Window was placed at E14.5. The embryonic regions depicted in panels L and M are indicated by the red and green squares. Scale bar, 2 mm. (**L**). 24-hour imaging of a NC chimeric embryo containing individual tdTomato+ mNCCs. (**M**). Imaging of a NC chimeric embryo containing individual GFP+ hNCCs, where the GFP signal was undetectable after 6 h. Scale bar, 100 μm.

Movie S1. Embryonic heartbeat, indicating that the embryos were still alive.

Movie S2. Pups were delivered normally and survived birth.

Movie S3. The dam fed the pups normally.

Movie S4. Imaging a whole Wnt1-cre:tdTomato mouse embryo from E11.5 to E11.75 using a stereoscopic microscope.

Movie S5. Synaptic transmission between neurons, imaged using the calcium indicator GCaMP.

Movie S6. Diffusion of fluorescein into an embryo at E15.5 following injection into the dam orbital vein.

Movie S7. Movement of cells in an embryo at E14.5, 24 h after *in utero* electroporation to introduce pCAG-mCherry.

Movie S8. Cell migration in an embryo at E15.5, 24 h after *in utero* electroporation to introduce pCAG-eGFP.

Movie S9. Continuous imaging of a whole chimeric embryo, injected with eGFP-labeled mESCs in blastocyst stage, for 12 h, from E11.5 to E12.0.

References

1. A. K. Hadjantonakis, M. E. Dickinson, S. E. Fraser, V. E. Papaioannou, Technicolour transgenics: imaging tools for functional genomics in the mouse. *Nat Rev Genet* **4**, 613-625 (2003). doi: 10.1038/nrg1126

2. A. Di Cristofano, B. Pesce, C. Cordon-Cardo, P. P. Pandolfi, Pten is essential for embryonic development and tumour suppression. *Nat Genet* **19**, 348-355 (1998). doi: 10.1038/1235

3. C. L. Gregg, J. T. Butcher, Quantitative *in vivo* imaging of embryonic development: opportunities and challenges. *Differentiation* **84**, 149-162 (2012). doi: 10.1016/j.diff.2012.05.003

4. P. Pantazis, W. Supatto, Advances in whole-embryo imaging: a quantitative transition is underway. Nat Rev Mol Cell Biol 15, 327-339 (2014). doi: 10.1038/nrm3786

5. K. McDole et al., *In Toto* Imaging and Reconstruction of Post-Implantation Mouse Development at the Single-Cell Level. Cell 175, 859-876 e833 (2018). doi: 10.1016/j.cell.2018.09.031

6. W. A. Munoz, P. A. Trainor, Mouse Embryo Culture for the Study of Neural Crest Cells. Methods Mol Biol 1976, 107-119 (2019). doi: 10.1007/978-1-4939-9412-0_9

7. M. N. Shahbazi, M. Zernicka-Goetz, Deconstructing and reconstructing the mouse and human early embryo. Nat Cell Biol 20, 878-887 (2018). doi: 10.1038/s41556-018-0144-x

8. K. E. Brett, Z. M. Ferraro, J. Yockell-Lelievre, A. Gruslin, K. B. Adamo, Maternal-fetal nutrient transport in pregnancy pathologies: the role of the placenta. Int J Mol Sci 15, 16153-16185 (2014). doi: 10.3390/ijms150916153

9. J. Cao et al., The single-cell transcriptional landscape of mammalian organogenesis. Nature 566, 496-502 (2019). doi: 10.1038/s41586-019-0969-x

10. C. Stremmel et al., Yolk sac macrophage progenitors traffic to the embryo during defined stages of development. Nat Commun 9, 75 (2018). doi: 10.1038/s41467-017-02492-2

11. A. Holtmaat et al., Long-term, high-resolution imaging in the mouse neocortex through a chronic cranial window. Nat Protoc 4, 1128-1144 (2009). doi: 10.1038/nprot.2009.89

12. L. Ritsma et al., Intravital microscopy through an abdominal imaging window reveals a pre-micrometastasis stage during liver metastasis. Sci Transl Med 4, 158ra145 (2012). doi: 10.1126/scitranslmed.3004394

13. N. Rakhilin et al., Simultaneous optical and electrical *in vivo* analysis of the enteric nervous system. Nat Commun 7, 11800 (2016). doi: 10.1038/ncomms11800

14. D. Entenberg et al., A permanent window for the murine lung enables high-resolution imaging of cancer metastasis. Nat Methods 15, 73-80 (2018). doi: 10.1038/nmeth.4511

15. G. A. Pilz et al., Live imaging of neurogenesis in the adult mouse hippocampus. Science 359, 658-662 (2018). doi: 10.1126/science.aao5056

16. N. Rakhilin et al., An intravital window to image the colon in real time. Nat Commun 10, 5647 (2019). doi: 10.1038/s41467-019-13699-w

17. J. Rinkenberger, Z. Werb, The labyrinthine placenta. Nat Genet 25, 248-250 (2000). doi:

10.1038/76985

18. A. P. McMahon, A. L. Joyner, A. Bradley, J. A. McMahon, The midbrain-hindbrain phenotype of Wnt-1-/Wnt-1- mice results from stepwise deletion of engrailed-expressing cells by 9.5 days postcoitum. Cell 69, 581-595 (1992). doi: 10.1016/0092-8674(92)90222-x

19. Y. Chai et al., Fate of the mammalian cranial neural crest during tooth and mandibular morphogenesis. Development 127, 1671-1679 (2000). pmid:10725243

20. X. Jiang, D. H. Rowitch, P. Soriano, A. P. McMahon, H. M. Sucov, Fate of the mammalian cardiac neural crest. Development 127, 1607-1616 (2000). pmid:10725237

21. K. Foster et al., Contribution of neural crest-derived cells in the embryonic and adult thymus. J Immunol 180, 3183-3189 (2008). doi: 10.4049/jimmunol.180.5.3183

22. F. Lin, Z. V. Wang, J. A. Hill, Seeing is believing: dynamic changes in renal epithelial autophagy during injury and repair. Autophagy 10, 691-693 (2014). doi: 10.4161/auto.27749

23. T. Kaizuka et al., An Autophagic Flux Probe that Releases an Internal Control. Mol Cell 64, 835-849 (2016). doi: 10.1016/j.molcel.2016.09.037

24. R. Gomez-Sintes et al., Standard Assays for the Study of Autophagy in the Ex Vivo Retina. Cells 6, (2017). doi: 10.3390/cells6040037

25. H. Tian et al., A reserve stem cell population in small intestine renders Lgr5-positive cells dispensable. Nature 478, 255-259 (2011). doi: 10.1038/nature10408

26. M. Yuryev et al., *In vivo* Calcium Imaging of Evoked Calcium Waves in the Embryonic Cortex. Front Cell Neurosci 9, 500 (2015). doi: 10.3389/fncel.2015.00500

27. N. J. Michelson, J. R. Eles, A. L. Vazquez, K. A. Ludwig, T. D. Y. Kozai, Calcium activation of cortical neurons by continuous electrical stimulation: Frequency dependence, temporal fidelity, and activation density. J Neurosci Res 97, 620-638 (2019). doi: 10.1002/jnr.24370

28. H. S. Leong et al., Intravital imaging of embryonic and tumor neovasculature using viral nanoparticles. Nat Protoc 5, 1406-1417 (2010). doi: 10.1038/nprot.2010.103

29. P. Wick et al., Barrier capacity of human placenta for nanosized materials. Environ Health Perspect 118, 432-436 (2010). doi: 10.1289/ehp.0901200

30. D. B. Cox, R. J. Platt, F. Zhang, Therapeutic genome editing: prospects and challenges. Nat Med 21, 121-131 (2015). doi: 10.1038/nm.3793

31. C. E. Nelson et al., Long-term evaluation of AAV-CRISPR genome editing for Duchenne muscular dystrophy. Nat Med 25, 427-432 (2019). doi: 10.1038/s41591-019-0344-3

32. A. K. Gruenert et al., Self-Complementary Adeno-Associated Virus Vectors Improve Transduction Efficiency of Corneal Endothelial Cells. PLoS One 11, e0152589 (2016). doi: 10.1371/journal.pone.0152589

33. M. dal Maschio et al., High-performance and site-directed in utero electroporation by a triple-electrode probe. Nat Commun 3, 960 (2012). doi: 10.1038/ncomms1961

34. J. Wu et al., Stem cells and interspecies chimaeras. Nature 540, 51-59 (2016). doi: 10.1038/nature20573

35. F. Soldner, R. Jaenisch, Stem Cells, Genome Editing, and the Path to Translational Medicine. Cell 175, 615-632 (2018). doi: 10.1016/j.cell.2018.09.010

36. M. A. Cohen et al., Human neural crest cells contribute to coat pigmentation in interspecies chimeras after in utero injection into mouse embryos. Proc Natl Acad Sci U S A 113, 1570-1575 (2016). doi: 10.1073/pnas.1525518113

37. R. Jaenisch, Mammalian neural crest cells participate in normal embryonic development on microinjection into post-implantation mouse embryos. Nature 318, 181-183 (1985). doi: 10.1038/318181a0

38. M. A. Cohen, S. Markoulaki, R. Jaenisch, Matched Developmental Timing of Donor Cells with the Host Is Crucial for Chimera Formation. Stem Cell Reports 10, 1445-1452 (2018). doi: 10.1016/j.stemcr.2018.03.004

39. T. Saito, *In vivo* electroporation in the embryonic mouse central nervous system. Nat Protoc 1, 1552-1558 (2006). doi: 10.1038/nprot.2006.276

40. L. J. Pilaz, A. L. Lennox, J. P. Rouanet, D. L. Silver, Dynamic mRNA Transport and Local Translation in Radial Glial Progenitors of the Developing Brain. Curr Biol 26, 3383-3392 (2016). doi: 10.1016/j.cub.2016.10.040

41. S. Markoulaki, A. Meissner, R. Jaenisch, Somatic cell nuclear transfer and derivation of embryonic stem cells in the mouse. Methods 45, 101-114 (2008). doi: 10.1016/j.ymeth.2008.04.002

42. Q. L. Ying et al., The ground state of embryonic stem cell self-renewal. Nature 453, 519-523 (2008). doi: 10.1038/nature06968

43. C. J. Lengner et al., Derivation of pre-X inactivation human embryonic stem cells under physiological oxygen concentrations. Cell 141, 872-883 (2010). doi: 10.1016/j.cell.2010.04.010

44. T. W. Theunissen et al., Systematic Identification of Culture Conditions for Induction and Maintenance of Naive Human Pluripotency. Cell Stem Cell 15, 524-526 (2014). doi: 10.1016/j.stem.2014.07.002

45. S. M. Chambers, Y. Mica, G. Lee, L. Studer, M. J. Tomishima, Dual-SMAD Inhibition/WNT Activation-Based Methods to Induce Neural Crest and Derivatives from Human Pluripotent Stem Cells. Methods Mol Biol 1307, 329-343 (2016). doi: 10.1007/7651_2013_59

46. Q. He et al., Sex-specific reference intervals of hematologic and biochemical analytes in Sprague-Dawley rats using the nonparametric rank percentile method. PLoS One 12, e0189837 (2017). doi: 10.1371/journal.pone.0189837